Supplementary Information

A 3D printed Cu evaporator support for record-high interfacial solar evaporation

Deyu Wang, Yiming Bu, Xuan Wu, Gary Owens, and Haolan Xu*[a]

Future Industries Institute, UniSA STEM, University of South Australia, Mawson Lakes Campus, Adelaide, SA 5095, Australia.

Email: haolan.xu@unisa.edu.au

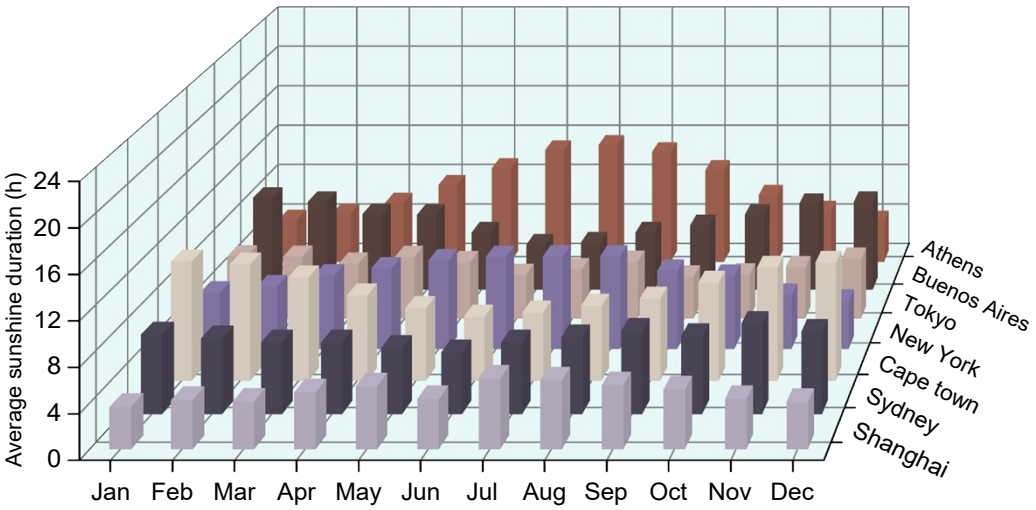

Figure S1. Average monthly sunshine duration across different major cities (Shanghai, New York, Sydney, Tokyo, Cape Town, Buenos Aires, and Athens)

Note S1. Selection of coastal cities

The selected coastal cities—Shanghai, New York, Sydney, Tokyo, Cape Town, Buenos Aires, and Athens—offer a comprehensive representation of global coastal climates due to their diverse geographical distribution and climatic variability. These cities encompass major climate classifications, including temperate monsoon (Shanghai, Tokyo), humid subtropical (Sydney), humid continental (New York), Mediterranean (Athens, Cape Town), and oceanic (Buenos Aires), effectively capturing the climatic diversity of the world's primary coastal urban centers. Their distribution across multiple continents and hemispheres, spanning various latitudes, ensures the inclusion of distinct solar radiation patterns and seasonal variations. Moreover, densely populated coastal megacities face increasing freshwater demand, which can be mitigated through desalination technologies, particularly in regions with high solar irradiance. Consequently, region-specific solar radiation data are essential for evaluating the feasibility and optimization of solar-powered desalination and other coastal energy applications.

Note S2. The definition of sunshine duration

World Meteorological Organization (WMO) defined sunshine duration: According to WMO (2003), sunshine duration during a given period is defined as the sum of that sub-period for which the direct solar irradiance exceeds 0.12 kW m^{-2}.

Note S3. Weather data sources

The weather data are sourced from the respective national meteorological websites of each country. Due to variations in local policies and data collection methods, the covered periods

differ across locations but generally span the past several decades.

Note S4. Sunlight intensity calculation

The solar radiation intensity at the surface can be calculated based on the solar elevation angle. The formula is:

$$G = G_0 \cdot sin(h)$$

$$h = arcsin[\sin(\emptyset) \cdot \sin(\delta) + \cos(\emptyset) \cdot \cos(\delta) \cdot \cos(\omega)]$$

$$\omega = 15 \cdot (T - 12)$$

$$\delta = 23.44 \cdot [\frac{360 \cdot (284 + N)}{365}]$$

Where G is the solar radiation intensity at the surface (in W/m²), G_0 is the solar constant (~1361 W/m²), h is the solar elevation angle (in degrees), $\emptyset$ is geographic latitude, δ is solar declination angle, ω is hour angle, T is the time (in hours, 24-hour format), N is the day of the year (1-365), and 23.44° is the earth's axial tilt.

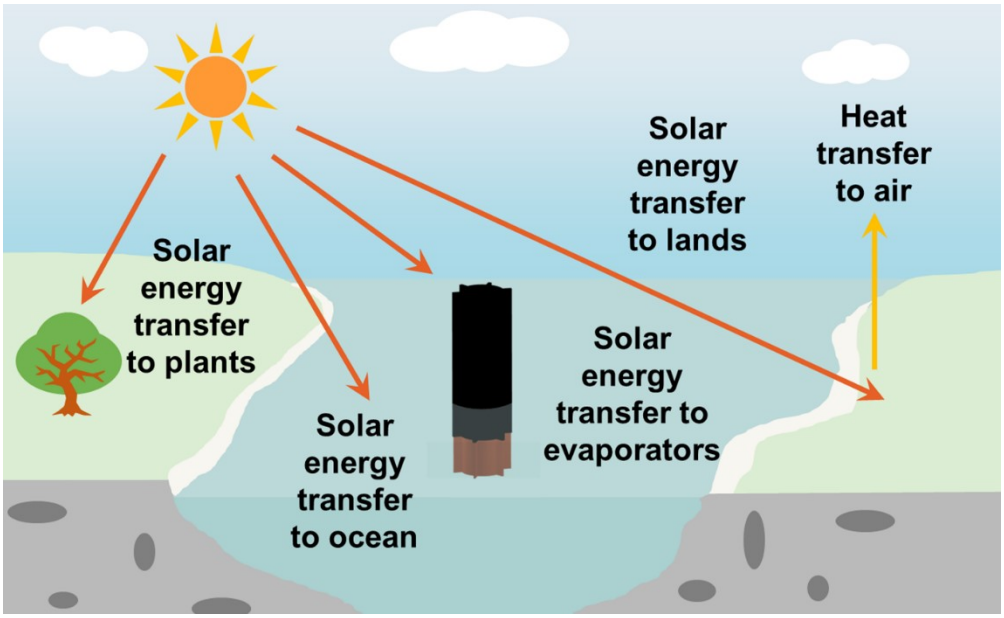

Figure S2. Schematic diagram of solar energy absorption and transfer among lands, ocean, plants, air and photothermal evaporators, illustrating the energy distribution and conversion process,

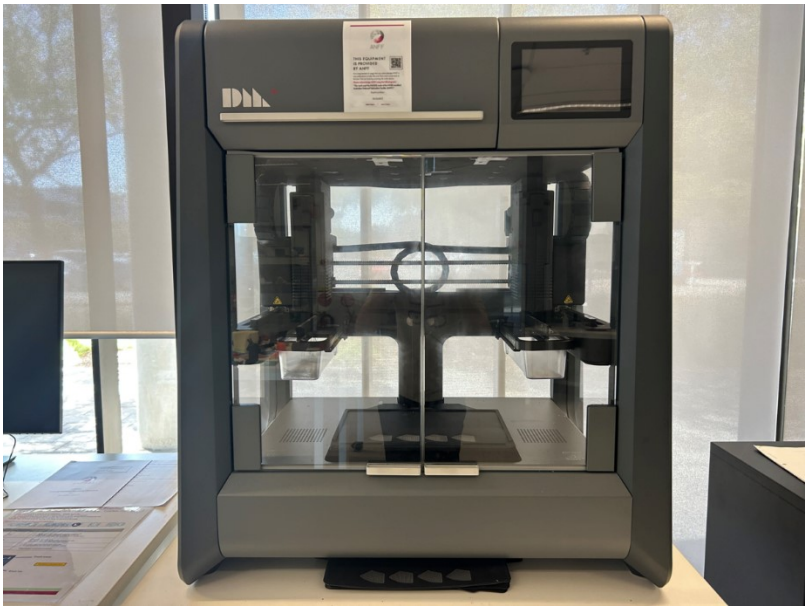

Figure S3. Photograph of a Desktop Metal Studio system BMD technology printer for 3D printing Cu.

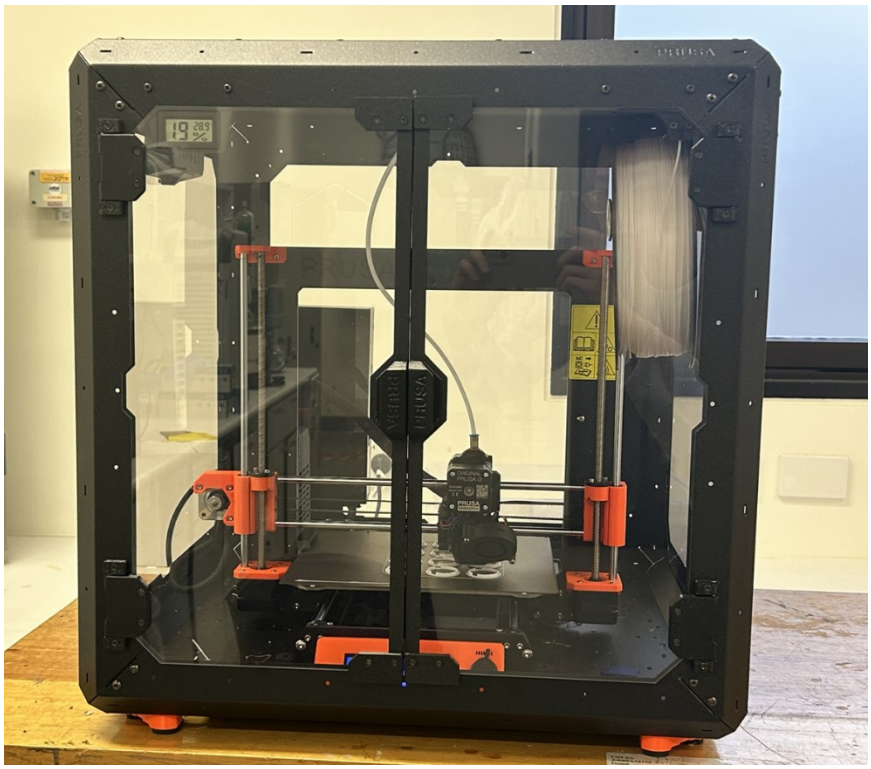

Figure S4. Photograph of Prusa i3 MK3S+ FDM printer for 3D printing PLA.

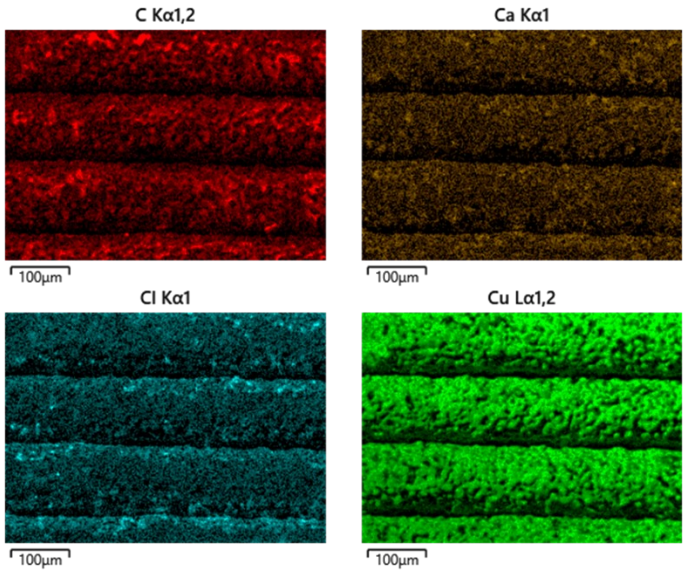

Figure S5. EDS elemental mapping of the PDA coated copper printing part after immersing in $CaCl_2$ solution.

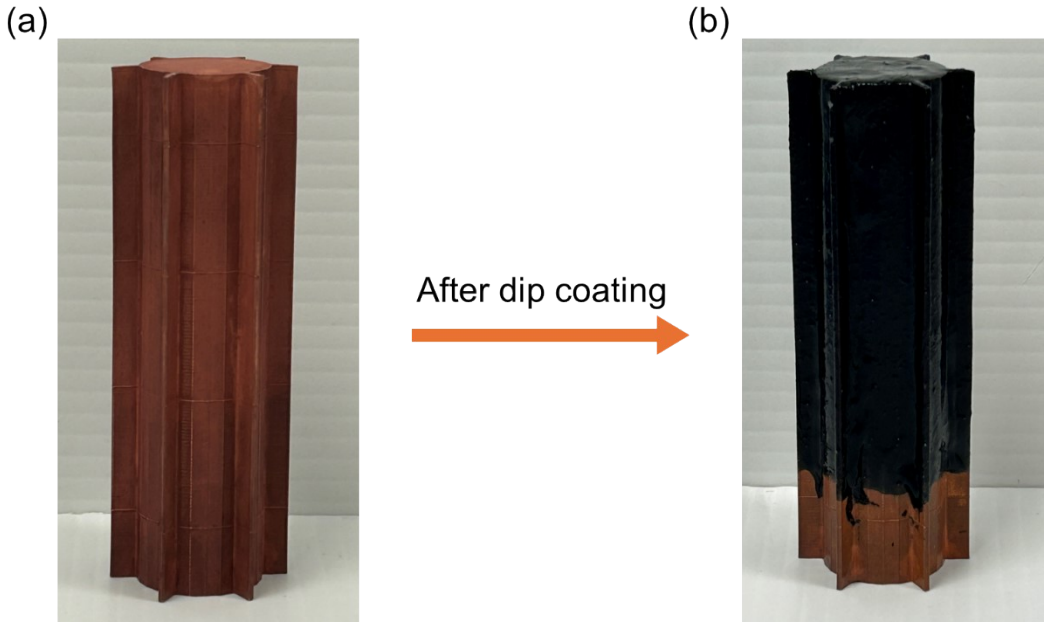

Figure S6. Digital photographs of (a) 3D printed Cu support, (b) PDA coated Cu support after dip-coating.

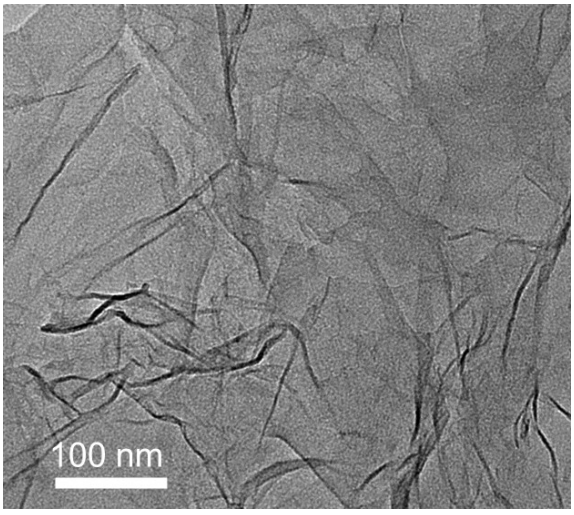

Figure S7. TEM image of the rGO nanosheet.

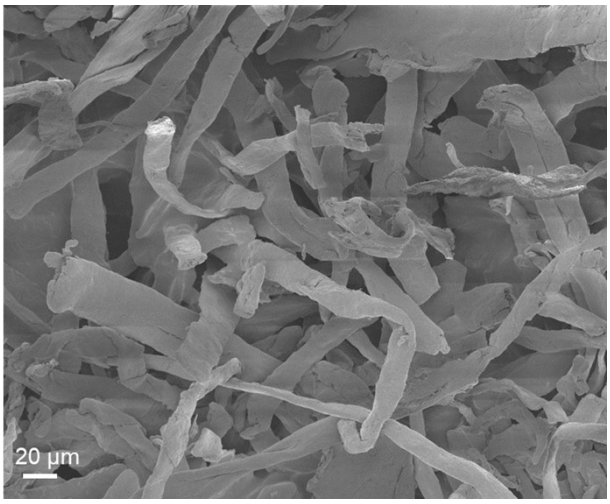

Figure S8. SEM image of the cellulose.

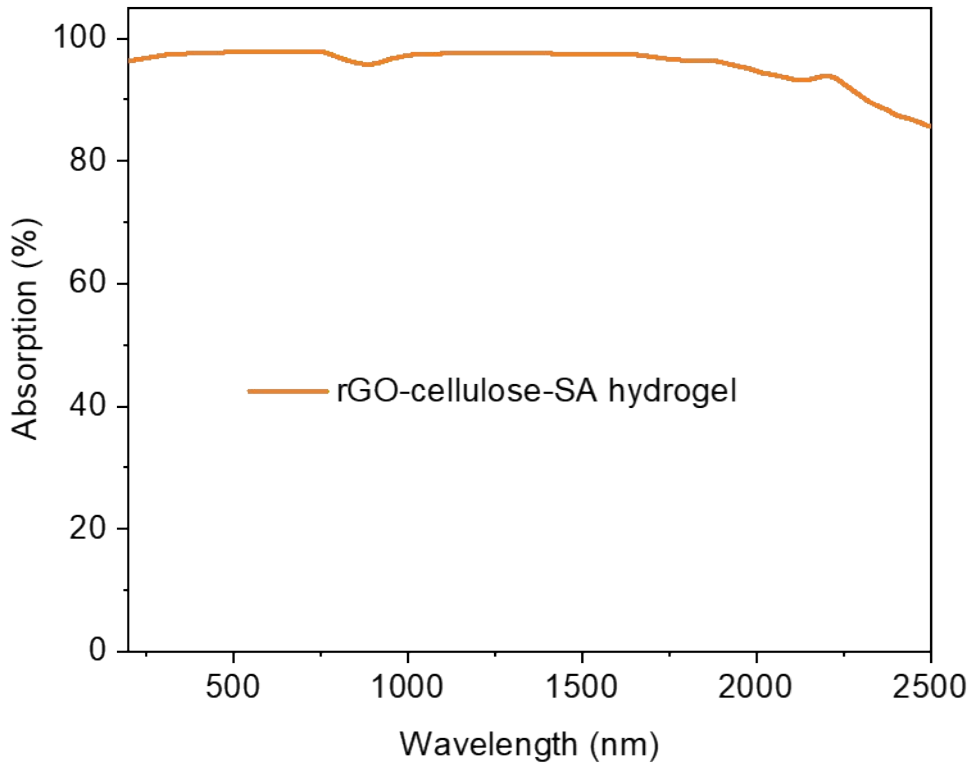

Figure S9. Absorbance spectra of the photothermal hydrogel.

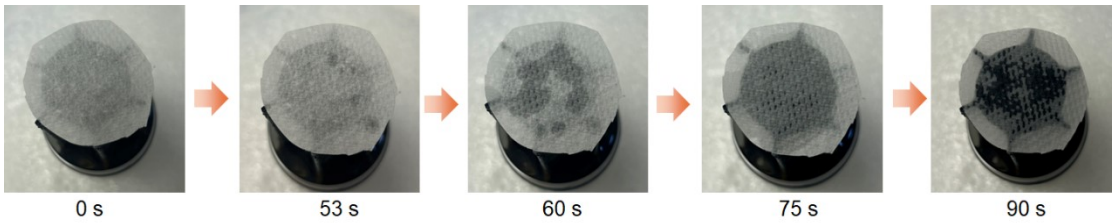

Figure S10. Photographs of the wetting process of a piece of paper placed on the top surface of the Cu-evaporator-6F, indicating water is transported to the top surface within 60 s.

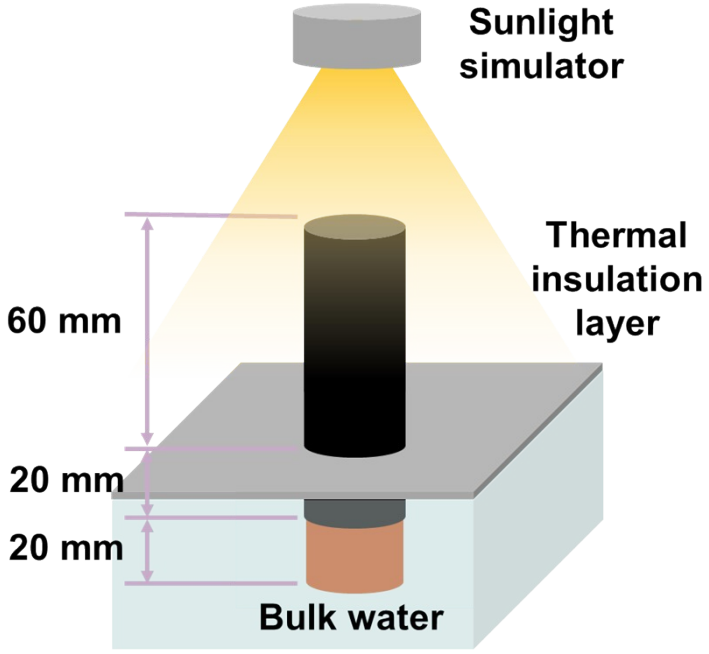

Figure S11. Schematic diagram of the evaporator setup during the solar or dark evaporation tests.

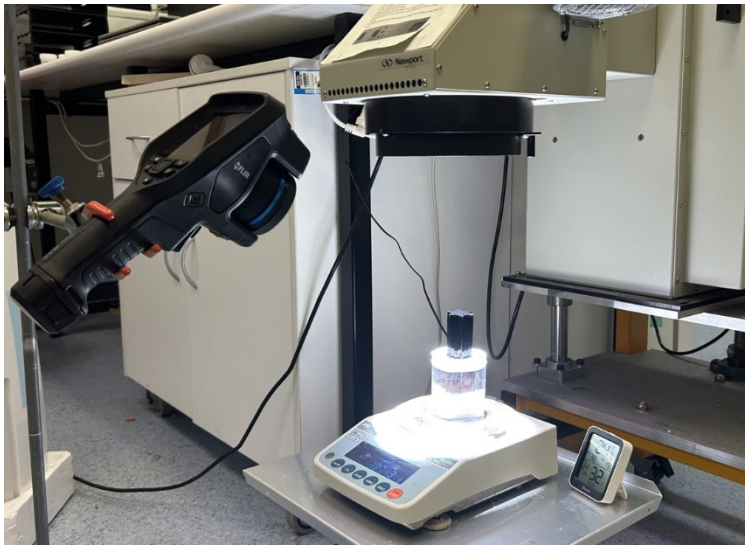

Figure S12. Photograph of the setup for solar evaporation tests using Newport Oriel solar simulator (69920) as light source and IR camera for surface temperature measurement.

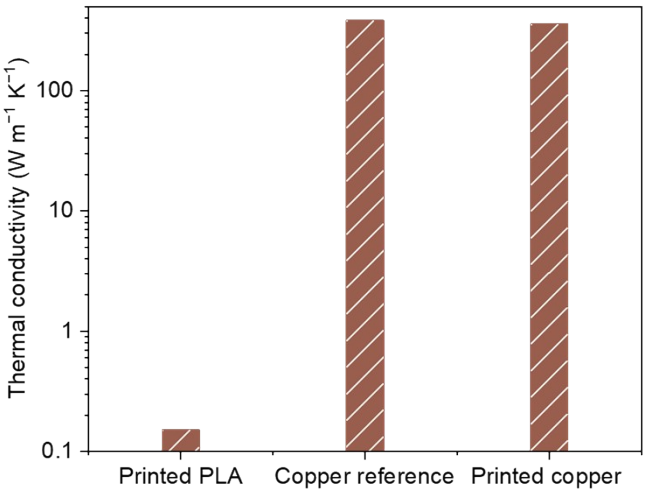

Figure S13. Thermal conductivity of PLA, commercial copper, and 3D printed copper.

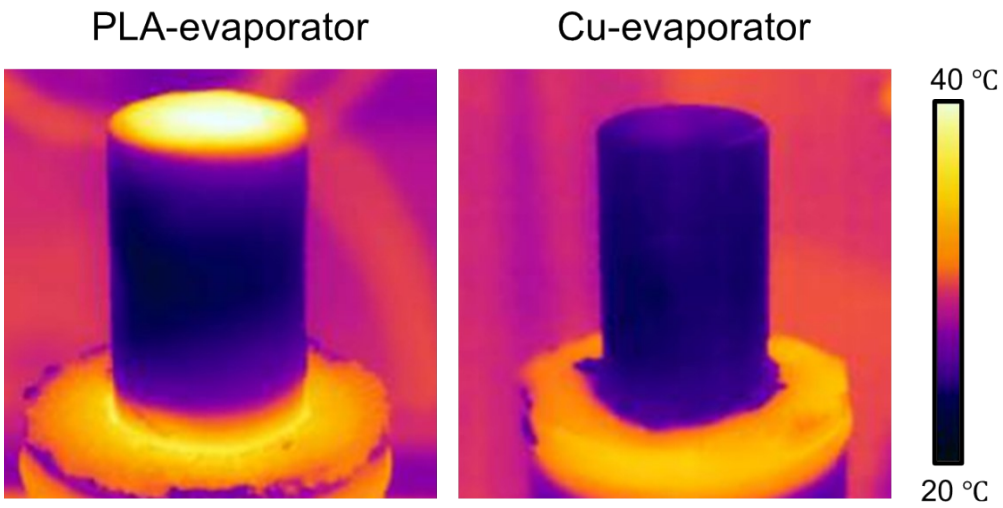

Figure S14. IR images of the PLA-evaporator and Cu-evaporator during the solar evaporation under 1.0 sun.

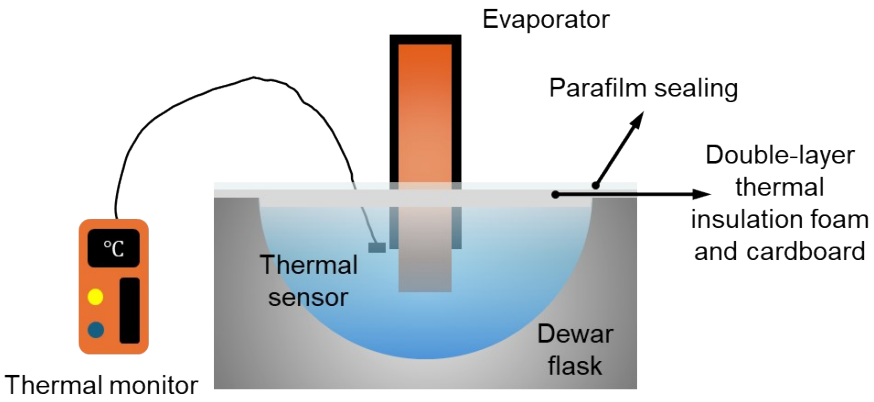

Figure S15. Schematic illustration of the thermal-insulation system during the solar evaporation test for bulk water temperature change monitoring.

To verify the ability of the Cu-evaporator to extract energy from bulk water, the PLA-evaporator and Cu-evaporator were placed in a thermally insulated system for solar evaporation tests. During the process, the temperature of bulk water within this thermally sealed system was continuously monitored. The change in bulk water temperature qualitatively reflects whether the evaporator can effectively extract thermal energy from the bulk water.

Figure S16. Photograph of the thermal-insulation system during the solar evaporation test for bulk water temperature change measurement.

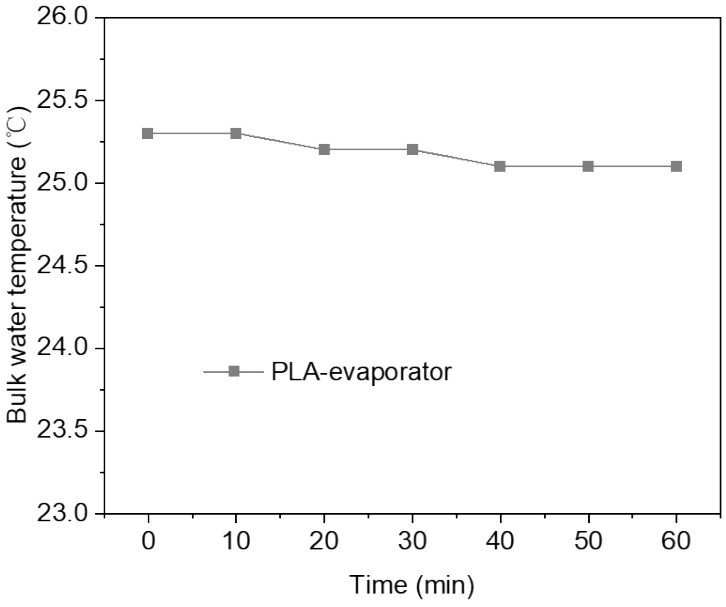

Figure S17. Bulk water temperature change in the thermal-insulation system with the PLA-evaporator.

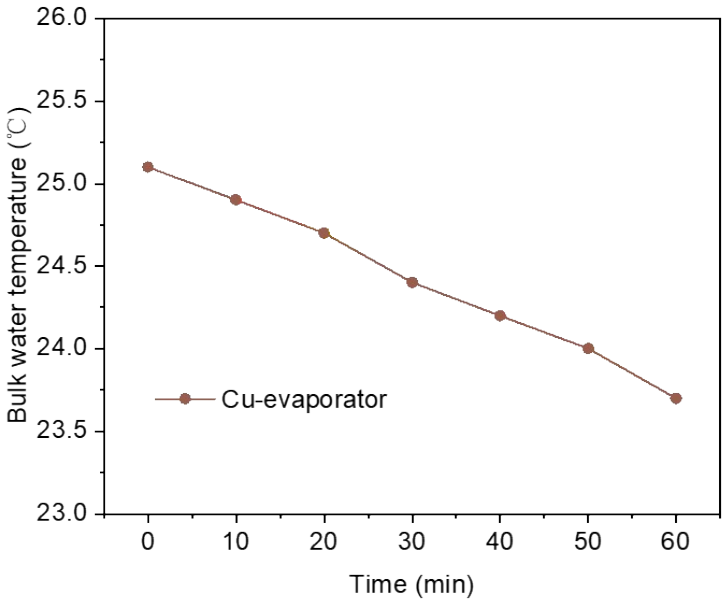

Figure S18. Bulk water temperature change in the thermal-insulation system with the Cu-evaporator.

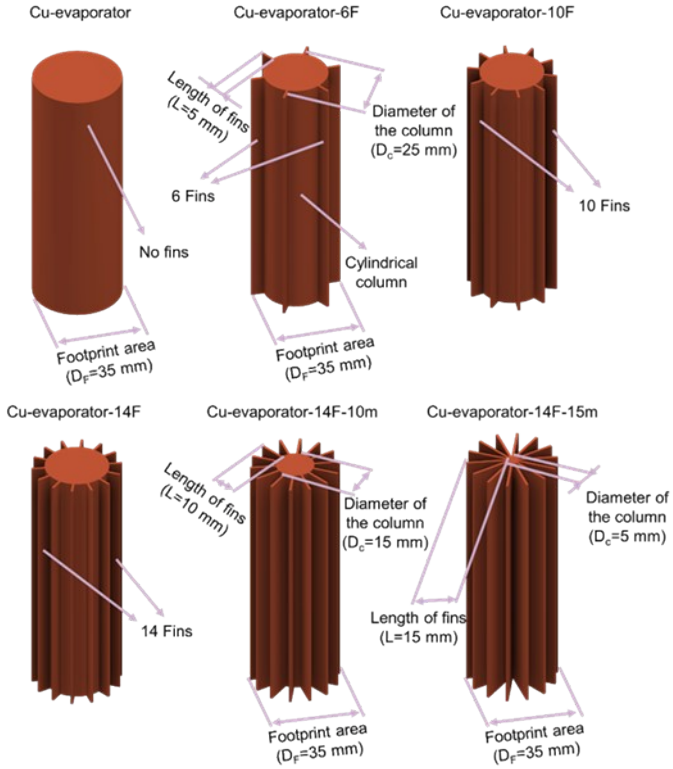

Figure S19. Geometrical scheme of all evaporators with different fin numbers and lengths.

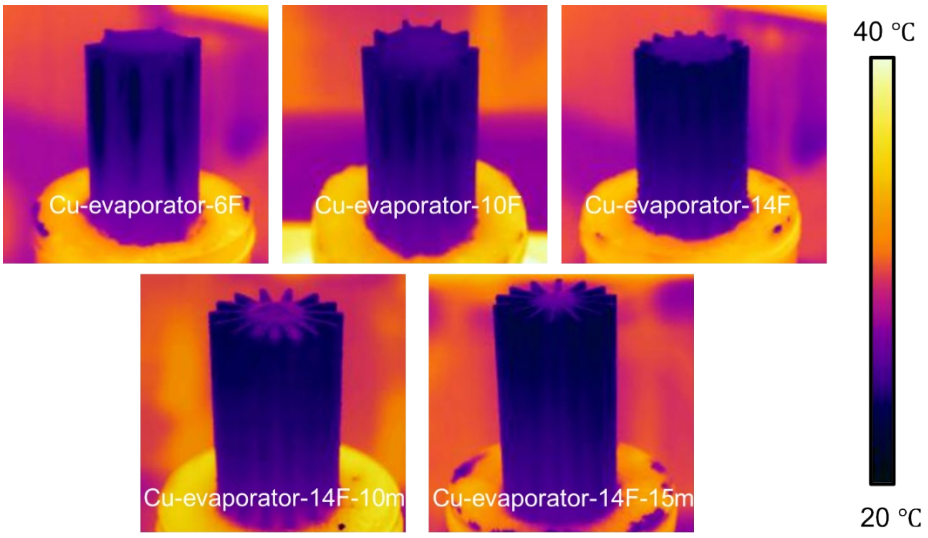

Figure S20. IR images of Cu-evaporators with various numbers and lengths of fins during solar evaporation processes.

Note S5. Calculation of energy inputs

Energy received from sunlight can be calculated by the formula:

$$P_{solar} = A_{top}\alpha E_{in}$$

Where P_{solar} is the solar energy input, A_{top} is the top surface area, α is the optical absorption coefficient of the photothermal surface (~0.95), E_{in} is the intensity of the solar radiation (1.0 kW m^{-2}).

Energy harvested from air can be calculated by the formula:

$$P_{radiation(air)} = A\varepsilon\sigma({T_{environment}}^4 - {T_{surface}}^4)$$

$$P_{convection(air)} = Ah_{air}(T_{environment} - T_{surface})$$

Where $P_{radiation}$ and $P_{convection}$ are the energy flux by radiation and convection, A_1 is

the area of the evaporation surface, ε is emissivity of the evaporation surface (~0.95), σ is the Stefan–Boltzmann constant (5.67×10^{-8} W m^{-2} K^{-4}), h_{air} is convection heat transfer coefficient of air (4 W m^{-2} K^{-1}), $T_{surface}$ and $T_{environment}$ represent the average evaporation surface temperature and the environment temperature during solar evaporation.

Energy extracted from bulk water $P_{conduction(water)}$ can be estimated using formula:

$$P_{conduction(water)} = \frac{k \cdot A \cdot (T_{bottom} - T_{up})}{L/2}$$

Where L is the evaporator height (60 mm), k is the thermal conductivity of the printed copper, A is the cross-sectional area of the copper supports, T_{bottom} is the temperature at the bottom of the evaporators, T_{up} is the temperature at the mid of the exposed evaporators.

Note S6. **Parameters used in conductive energy harvesting from bulk water calculation**

The process of energy extraction from bulk water can be simplified as steady-state heat conduction between the bottom part of the evaporator that immersed in bulk water and the upper part that exposed to the air for water evaporation. The interface between the two parts was treated as the entry point of heat flow. The energy transfer between the two parts can be reasonably approximated using Fourier's law. The parameters at the geometric center of the evaporation part can be reasonably used to represent the average thermal state of the region. Given the extremely thin nature of the evaporation layer, the overall thermal conductivity of the evaporator is approximated by that of 3D-printed copper.

Note S7. Enthalpy of evaporation test

The evaporation enthalpy of water in rGO-Cellulose-SA hydrogel was tested for calculating the energy required for water evaporation. The same surface area of bulk water and water in rGO-cellulose-SA hydrogel were placed in a closed container together with a supersaturated magnesium chloride solution (maintaining a stable RH of 33%) at 25 ºC. Mass losses were recorded after 90 mins. The equivalent evaporation enthalpy (ΔH_{equ}) of bulk water and water in hydrogel were calculated by the following equation:):

$\Delta H_0 m_0 = \Delta H_{equ} m_g$

where ΔH_0 and m_0 are the evaporation enthalpy and mass loss of bulk water; m_g is the mass loss of hydrogel-water.

The calculated evaporation enthalpy of water in rGO-Cellulose-SA hydrogel is 1729.39 kJ kg^{-1}.

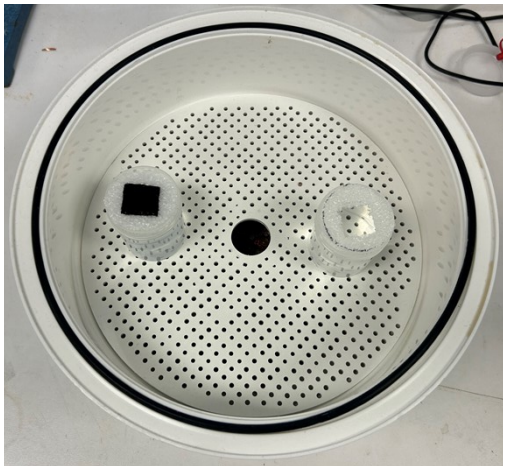

Figure S21. Photograph of the evaporation enthalpy test by dark evaporation experiments.

Note S8. COMSOL Simulation.

Numerical simulations were conducted using the COMSOL Multiphysics 6.1. Multi-modules

combining Laminar Flow and Heat Transfer in fluid and solid were applied to simulate the generated vapor diffusion pattern and energy extraction from bulk water during solar evaporation. The intensity and the direction of vapor diffusion and energy transportation could be reflected via the simulated magnitude and direction of the arrows. Since vapor is generated from the evaporating surface, it will naturally diffuse into the air due to the humidity difference, a process that is consistent with laminar flow. The velocity field could be described as the following equations:

$$\rho\frac{\partial u}{\partial t} + \rho(u \cdot \nabla)u = \nabla \cdot [-pI + K] + \rho g$$

$$\frac{\partial \rho}{\partial t} + \nabla \cdot (\rho u) = 0$$

Where g is the acceleration coefficient of gravity; I is the constitutive relation coefficient and K is the fluid viscosity. Except for the vectorial velocity field (u) determined by heat flow, the variables were only moisture air density (ρ) in this node. In a short-period simulation, the variation of moisture air density could be neglected. Thus, the process was simplified to conduct a convection evaluation.

In this regard, heat transfer nodes can demonstrate the heat transfer process during solar evaporation. The dynamic physical process of heat transfer in solid was illustrated as:

$$\rho C_p u \cdot \nabla T + \nabla \cdot q = Q$$

$$q = -k\Delta T$$

ρ is the density; C_p is the specific heat capacity, u is the velocity field of the fluid, ΔT is the temperature gradient, q is the heat flux density, $\nabla \cdot q$ is the divergence of heat flux, Q is the internal heat source, and k is the thermal conductivity.

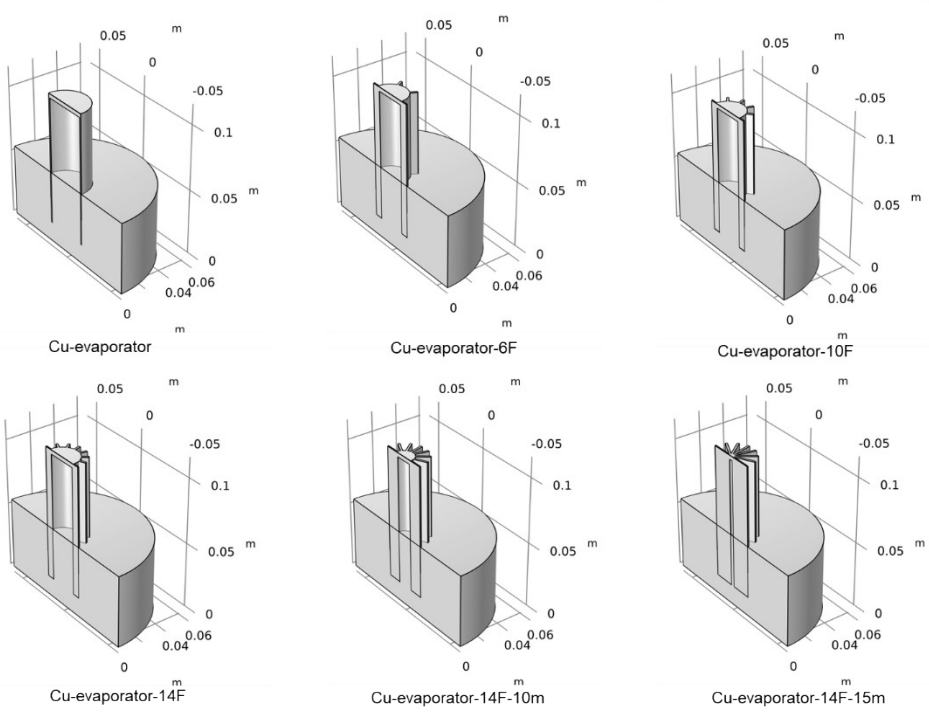

Figure S22. Detailed model geometries of the evaporators used in numerical simulations.

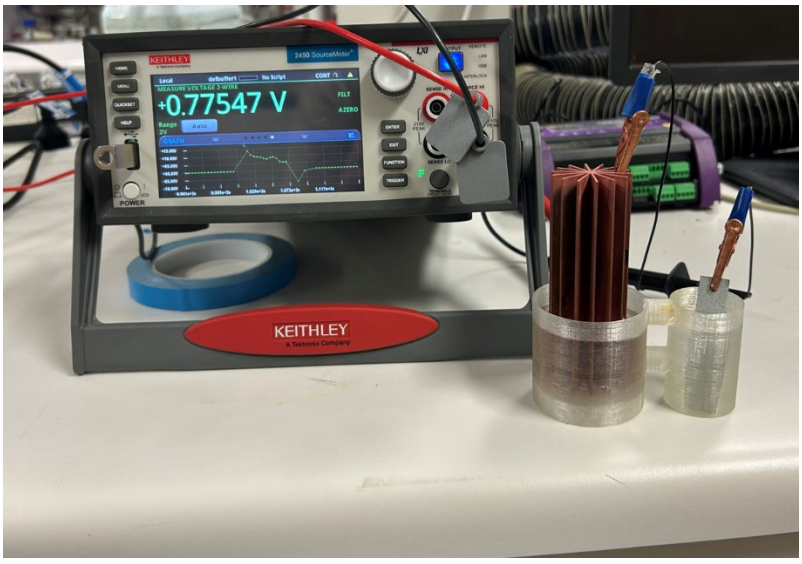

Figure S23. Setup for open-circuit voltage output and short-circuit current test using Keithley

source meter unit (2450).

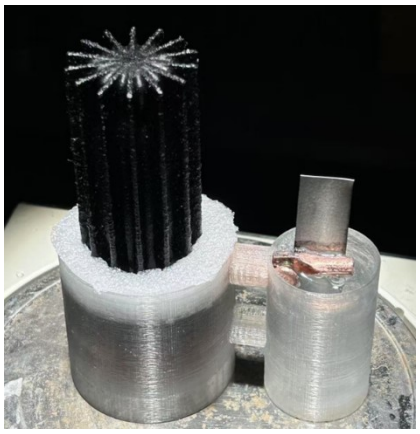

Figure S24. Digital photographs of the Cu-evaporator-14F-15m evaporator equipped with the corrosion protection system during solar evaporation of real seawater.

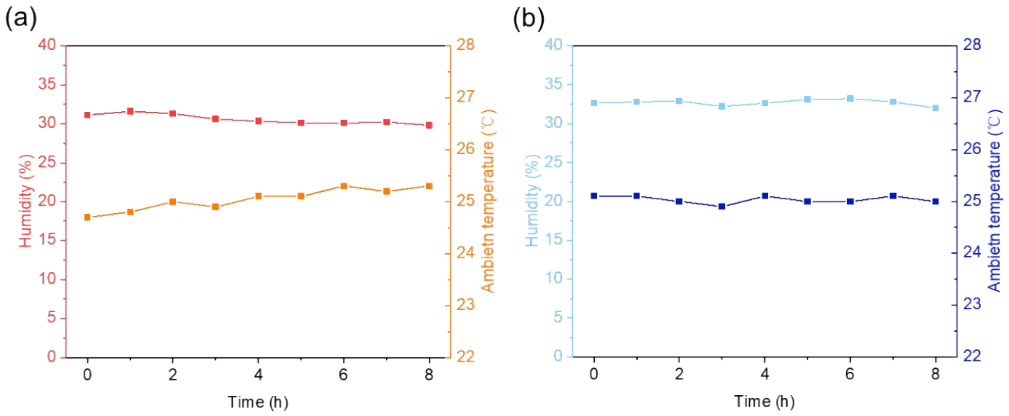

Figure S25. Ambient temperature and humidity during (a) solar and (b) dark evaporation tests with Cu-evaporator-14F-15m.

Figure S26. Photograph of Cu-evaporator-14F-15m after 8 hours solar evaporation test in real seawater. There is no salt accumulation on the surface.

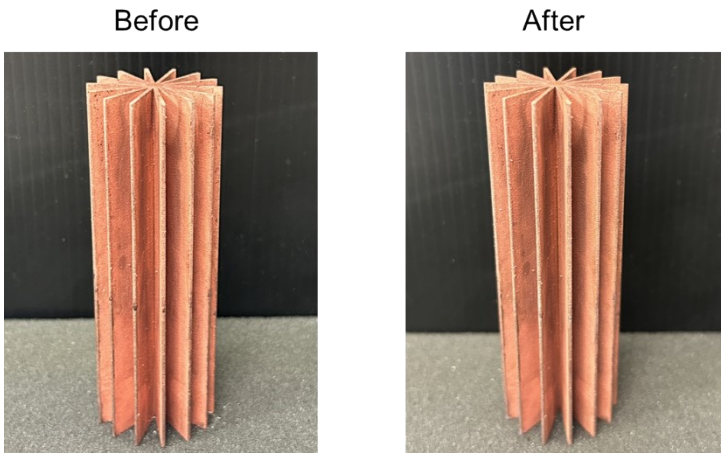

Figure S27. Photograph of the copper support after 8 hours of solar evaporation test in real seawater. There is no corrosion on the surface.

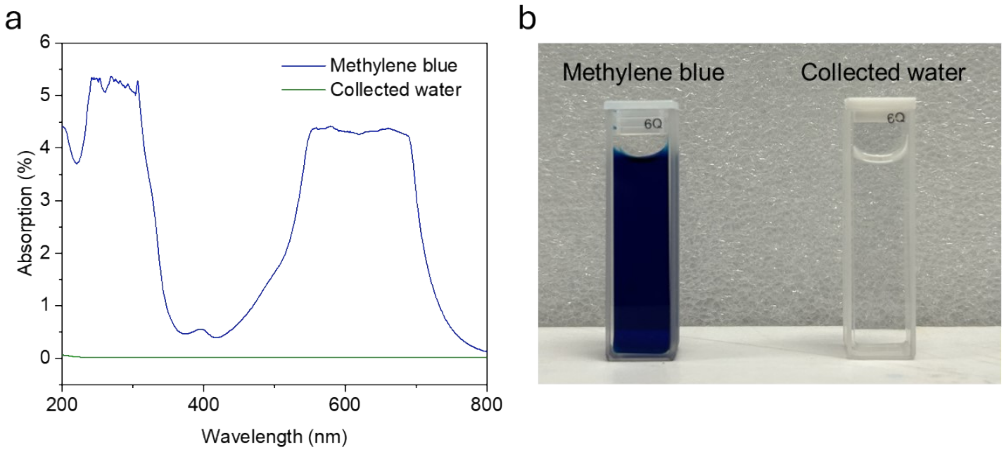

Figure S28. (a) Absorption spectrum of methylene blue solution and the collected water after solar evaporation, (b) photograph of the methylene blue solution and the collected water.

Table S1. Summary of energy input and evaporation performance for Cu-evaporators with different fin structures.

	Cu-evaporator	Cu-evaporator-6F	Cu-evaporator-10F	Cu-evaporator-14F	Cu-evaporator-14F-10m	Cu-evaporator-14F-15m	
Diameter of the project area (mm)	35	35	35	35	35	35	

Diameter of the central cylinder (mm)	35	25	25	25	15	5
Length of the fins (mm)	0	5	5	5	10	15
Top surface area (mm^2)	962.11	520.87	540.87	560.87	394.47*	273.62*
Side surface area (mm^2)	6597.34	8312.39	10712.39	13112.39	19627.43	26142.48
Top surface temperature (℃)	24.50	23.60	23.70	23.50	23.80	23.70
Side surface temperature (℃)	23.70	23.10	23.20	22.60	22.70	22.30
Bot surface temperature (℃)	25.20	25.10	25.20	24.60	24.50	23.90
Solar energy input (W)	0.91	0.49	0.51	0.53	0.37	0.26
Radiation energy gain of side surface from the air (W)	0.07	0.09	0.12	0.19	0.30	0.53

Radiation energy gain of top surface from the air (W)	0.01	0.01	0.01	0.01	0.00	0.00
Convection energy gain of side surface from the air (W)	0.03	0.05	0.06	0.11	0.17	0.32
Convection energy gain of top surface from the air (W)	0.01	0.01	0.01	0.01	0.01	0.00
Total energy gain from the air (W)	0.12	0.15	0.20	0.32	0.48	0.86
Conductive energy gain of from the bulk water (W)	1.90	2.51	2.98	3.46	3.94	4.23
Calculated total energy input (W)	2.94	3.15	3.70	4.31	4.79	5.36
Mass change (g)	6.00	6.92	8.05	8.80	9.40	10.72
Evaporation rates (kg m^{-2} h^{-1})	6.24	7.20	8.37	9.15	9.78	11.15
Evaporation energy request (W)	2.88	3.32	3.87	4.23	4.52	5.15

Ratio of calculated energy input and evaporation energy request	1.02	0.95	0.96	1.02	1.06	1.04

* The thickness of the surface coating is significant for these samples due to their inherently small top surface areas. As a result, the reported top areas are slightly larger.